Low-threshold photonic crystal laser

Marko Loncar, Tomoyuki Yoshie, Yueming Qiu, Pawan Gogna, Axel Scherer

Marko Loncar, Tomoyuki Yoshie, Yueming Qiu, Pawan Gogna, Axel Scherer, "Low-threshold photonic crystal laser," Proc. SPIE 5000, Photonic Crystal Materials and Devices, (9 July 2003); doi: 10.1117/12.472818

SPIE.

Event: Integrated Optoelectronics Devices, 2003, San Jose, CA, United States

Low-threshold photonic crystal laser

Marko Lončar[a], Tomoyuki Yoshie[a], Yueming Qiu[b], Pawan Gogna[b] and Axel Scherer[a]

[a]Nanofabrication Group, California Institute of Technology, 136-93, Pasadena, CA 91125
[b]In Situ Technology and Experiments Systems Section, Jet Propulsion Laboratory, California Institute of Technology, MS 302-306, Pasadena, CA 91109

ABSTRACT

We have fabricated planar photonic crystal nanocavity lasers based on our high quality-factor design that incorporates fractional edge dislocations in triangular lattice photonic crystal cavities. Lasers with InGaAsP quantum well active material emitting at 1550nm were optically pumped with 10ns pulses, and lase at room temperature at threshold pumping powers below 220μW. We have attributed this to the small mode volume and high Q factors inherent to our device design. We have performed detailed numerical analysis of our structures, and have found an excellent agreement between theoretical predictions and experimental results. The optical field of the lasing mode in our nano-laser is localized in the air-hole region and therefore the laser can be used to investigate interaction between light and matter introduced in the cavity and nanospectroscopy.

Keywords: p hotonic crystals, photonic bandgap, semiconductor lasers, InGaAsP

1. INTRODUCTION

Photonic crystals, often referred to as a "semiconductor for light", are recent innovation that can permit the miniaturization of integrated optical circuits to a scale comparable to the wavelength of light. These man-made periodic nano-structures, with high refractive index contrast modulation, can be designed to open up frequency bands (photonic band-gap) within which the propagation of electromagnetic waves is forbidden irrespective of the propagation direction. One class of photonic crystals, planar photonic crystals (PPC), represents particularly promising geometry for realization of compact nano-optical devices and their integration with microelectronic devices due to compatible fabrication techniques of the two systems. The basis of the planar photonic crystal is a dielectric slab, perforated with a two dimensional periodic lattice of holes.[1,2] The light is localized to the slab in the vertical direction by means of total internal reflection and is controlled in the lateral direction by distributed Bragg reflection due to the presence of 2D lattice of holes. The combination of these two mechanisms makes localization of light in all three dimensions possible. One of the most promising applications of planar photonic crystals is realization of compact and efficient optical nano-cavity, with high quality factor (Q) and small mode volume (V_{mode}). Many theoretical treatments of photonic crystal cavities have been reported, structures were successfully realized in various material systems, high quality factor (Q) designs have been proposed and experimentally verified and room-temperature lasing was reported by several groups.[3–15]

In this work we report theoretical and experimental analysis of high-Q optical nano-cavities based on triangular lattice planar photonic crystal. Cavity design is based on *fractional edge dislocations* in single defect PPC cavity (Figure 1). In our earlier publications we predicted high quality factors ($Q > 10,000$) in these structures,[5,16] demonstrated low-threshold room temperature lasing,[14] and measured record-high quality factors.[8] Here we present in-depth theoretical analysis of cavities based on fractional edge dislocations and compare theoretical predictions with experimental results. The paper is organized as follows: in section 2 we present results of 3D finite difference time domain (3D FDTD) analysis; wafer design and nanofabrication procedure is reported in section 3; experimental results are described in section 4; conclusions and discussion of the results are summarized in section 5.

Send correspondence to loncar@caltech.edu

Photonic Crystal Materials and Devices, Ali Adibi, Axel Scherer, Shawn Yu Lin, Editors,
Proceedings of SPIE Vol. 5000 (2003) © 2003 SPIE · 0277-786X/03/$15.00

2. STRUCTURE DESIGN AND FINITE DIFFERENCE TIME DOMAIN ANALYSIS

The structure that we are interested in is based on a single defect cavity defined in a triangular lattice planar photonic crystal. Our planar photonic crystal is based on a free-standing membrane: high dielectric constant slab (refractive index $n = 3.4$) is perforated with 2D lattice of holes with periodicity a and is suspended in the air. The cavity consists of a defect hole (radius r_{def}) that is smaller than surrounding holes (radius r) which define the photonic crystal mirror. The row that contains the defect hole is elongated by moving two photonic crystal half-planes a fraction of a lattice constant apart in the ΓX direction (Figure 1). Each half-plane is moved by $p/2$, yielding total dislocation of p.

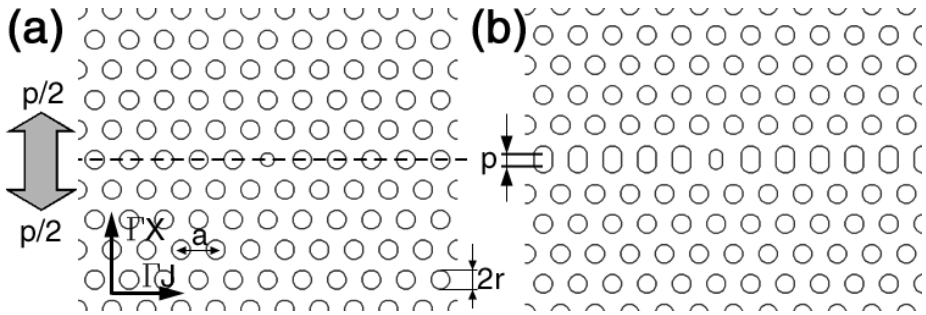

Figure 1. (a) Conventional single defect cavity ($p = 0$). When structure is "cut" along the dashed line, and two PPC half-planes are dislocated along ΓX direction by $p/2$, (b) high-Q cavity can be formed ($p = 0.25 \cdot a$).

In our earlier publication[5] we showed that in photonic crystal cavities, with $r/a = 0.275$, $r_{def}/a = 0.2$ and $d/a = 0.75$ (d is thickness of the slab), it is possible achieve Q factors as high as 11,000 by tuning the dislocation parameter p. The Q was maximized when $p/a = 10\%$. These high Q values were obtained while maintaining a very small mode volume of $V_{mode} \approx 0.1(\lambda/2)^3$. The cavities described in Reference 5 were originally designed for cavity QED experiments, where strong-coupling between atoms introduced into the high field region of the cavity and light trapped in the cavity is to be investigated. However, it is clear that the presence of a hole at the point of maximum field intensity is not desirable in low-threshold laser designs, since the overlap with the gain region is decreased. Therefore, we have revisited the problem of cavity design in order to investigate the influence of the defect hole size (r_{def}) on the Q factor of the cavity.

In order to improve the lateral confinement of light, we decided to analyze structures with slightly bigger holes ($r/a = 0.3$). This results in more compact cavity, since fewer layers of photonic crystal can be used to efficiently confine the light. On the other hand, bigger holes in the photonic crystal mirror increase the scattering of light in the vertical direction and therefore result in decreased Q factors. As the first step, we calculated the band diagram of the bulk photonic crystal with parameters $r/a = 0.3$, $d/a = 0.75$, and $n_{slab} = 3.4$, and we found that bandgap exists for vertically even modes (TE-like) for the normalized frequencies in the range $a/\lambda \in (0.2508, 0.3329)$. 3D FDTD was used to calculate this dispersion diagram, as described in Reference 17. The discretization used in FDTD algorithm was $a = 20$ computational points. Next, we modelled various high-Q cavity designs in order to find their eigen-modes. In Figure 2 we show the results of 3D FDTD analysis of the structure with $p/a = 10\%$, $r_{def} = 0.2a$, $r = 0.3a$ and $d = 0.75a$. Two dipole modes, labelled LQ and HQ, are found to exist in the cavity. These dipole modes correspond to doubly-degenerate modes of the simple single defect cavity,[3] but the degeneracy between them is lifted due to the dislocation. Also, additional modes are found close to the air-band. Those modes are not localized to the defect hole, but are instead attributed to the waveguide modes of the elongated central row.

As the next step, we investigated the dependence of the frequency of the two modes on the geometry of the cavity. Figure 3 shows positions of the two dipole modes as the function of elongation (p) and the size of the defect hole (r_{def}). It can be seen that in all cases two dipole modes are more split-apart as the dislocation increases. This is due to the fact that the modes interact more strongly (they are not orthogonal anymore) as p is increased. On the other hand, as the defect hole becomes bigger, the modes are shifted towards higher

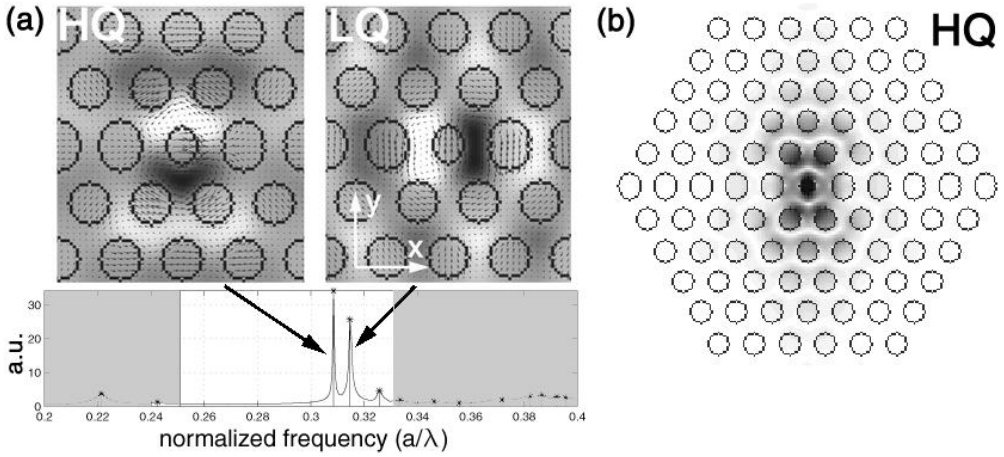

Figure 2. Defect modes of the cavity with $p/a = 10\%$ and $r_{def} = 0.2a$. (a) Cavity supports two dipole modes, and their profiles are shown (B_z component and vector of the $\vec{E}$ field). Gray shaded region in the spectrum corresponds to the modes of the bulk photonic crystal, while the bandgap is represented with white color. (b) Amplitude of the E field is shown. It can be seen that light is localized in the small defect hole.

frequencies. This is expected since modes' overlap with the low-dielectric constant material (air) increases as r_{def} increases. One more interesting feature is that splitting between LQ and HQ modes does not depend strongly on the size of the central hole, and is mostly dependant on the amount of dislocation introduced.

For fixed r_{def} mode with smaller eigen-frequency (HQ) has higher quality factor than the other mode (LQ).

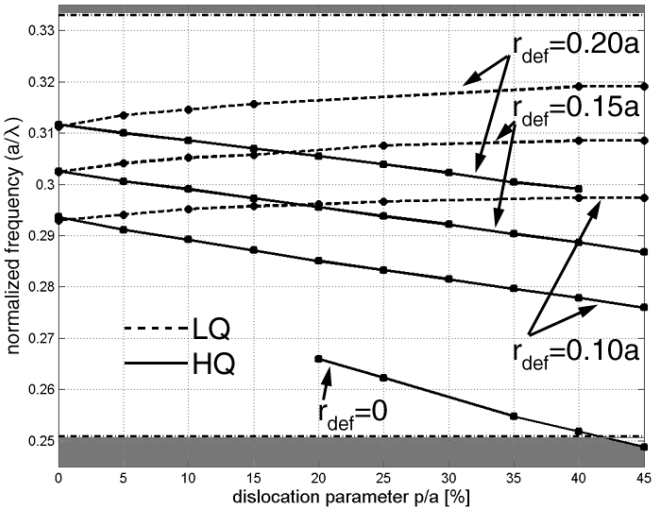

Figure 3. Dependence of the position of the two dipole modes of the cavity on the amount of dislocation introduced (p), and the size of the defect hole (r_{def}).

Therefore, the mode of interest is the HQ mode, the one that has $\vec{E}$ field aligned along x-axis, as shown in Figure 2(a). The quality factors of LQ modes are limited to several hundreds and therefore are not of practical importance. In Figure 4 we show dependence of the vertical (Q_{vert}) and lateral ($Q_{lateral}$) quality factors of the HQ mode on the amount of fractional edge dislocation introduced (p), for various sizes of central defect

hole (r_{def}). For definition of lateral and vertical Q-factors interested reader can see Reference 3. The lateral Q-factor (in-plane Q-factor) depends on the position of the mode within the bandgap, and can be improved by adding more photonic crystal layers around the cavity. The ultimate Q-factor that we can achieve is therefore limited by Q_{vert}. In our calculations, cavity was surrounded with five layers of photonic crystal, as shown in Figure 2(b).

The highest Q-factor that we could achieve in our cavities is around 7,000, when $r_{def}/a = 0.2$. For com-

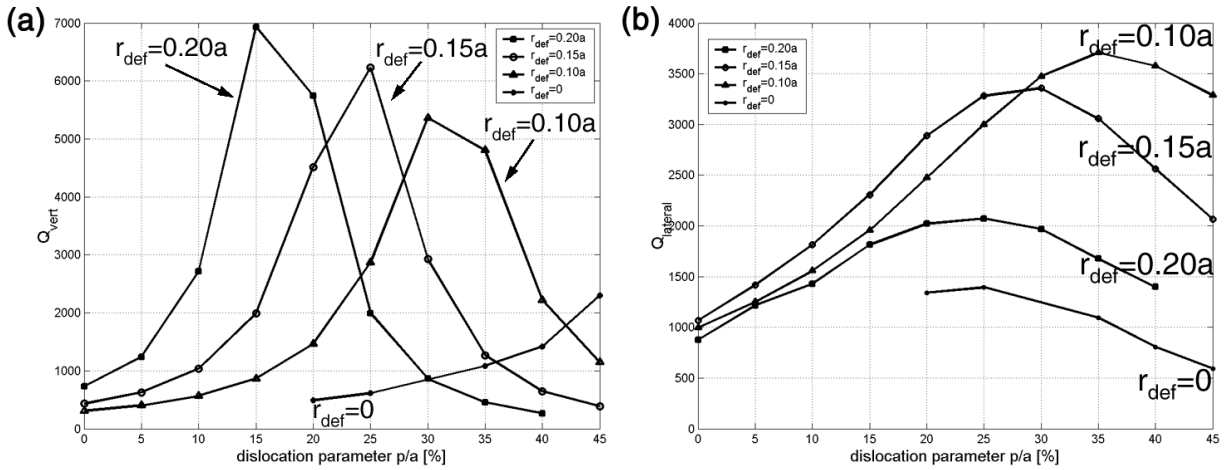

Figure 4. Dependence of the (a) vertical and (b) lateral quality factor of the HQ mode on the amount of dislocation (p) and the size of the defect hole (r_{def}). Only five layers of photonic crystal surrounding the defect hole was used. $Q_{lateral}$ can be improved by adding more photonic crystal layers.

parison, we were able to achieve Qs as high as 11,000 when $r/a = 0.275$.[5] As expected, bigger holes of the bulk photonic crystal used in the present work ($r/a = 0.3$) introduce more scattering of light, and therefore the Q-factors are smaller. Another important conclusion is that Q-factors higher than 5,000 can be achieved even when the central defect hole is made smaller. However, optimal design (Q-factor maximized) requires more dislocation as r_{def} decreases. This can be understood and explained by performing Fourier analysis of the HQ mode field components as described in our earlier publication.[16] For example, when $r_{def} = 0.1a$, $Q_{vert} \approx 5,500$ can be achieved if $p/a = 30\%$. This is important result for realization of low-threshold lasers since both reduced r_{def} and increased p/a will increase overlap between the eigen-mode of the cavity and gain (dielectric) region, thus reducing the threshold powers. However, in our design we still want to keep the central defect hole since the application that we have in mind for our lasers is nano-spectroscopy, and interaction between cavity field and matter introduced into the defect hole is of interest. For example, our device could be used as an efficient and compact gas sensor.

3. FABRICATION PROCEDURE

Our cavities were fabricated in InGaAsP quantum well material. Metalorganic chemical vapor deposition was used to grow the active laser structure on an InP substrate. Optical gain is provided by four $9nm$ thick, compressively strained, quantum wells with an electronic bandgap at $E_g = 1.55\mu m$, separated by $20nm$ thick InGaAsP barriers ($E_g = 1.22\mu m$). This active material is placed in the center of a $330nm$ thick InGaAsP slab ($E_g = 1.22\mu m$), with $1\mu m$ thick sacrificial InP layer underneath the slab. An InGaAs etch stop is introduced above the InP substrate, and the active quaternary material is designed to operate at $\lambda = 1.55\mu m$. Because of the compressive strain, the coupling is the strongest to the TE polarized modes of the slab. This is desirable since in triangular lattice PPC the bandgap is larger for TE-polarized light. An etch mask consists of $40nm$ Au evaporated on top of $100nm$ SiON, deposited using plasma-enhanced chemical vapor deposition. The fabrication

process starts with the deposition of $150nm$ of polymethyl methacrylate (PMMA) electron beam resist, followed by electron-beam lithography to define structures in PMMA. We use an Ar^+ ion milling step to transfer the mask pattern through the Au metal mask, and this procedure is followed by a C_2F_6 reactive ion etching (RIE) to transfer the mask from the Au into the SiON. Inductive-coupled plasma RIE etching is finally used to transfer the pattern from the SiON mask layer into the InGaAsP. Finally, the mask is removed in a HF acid and the InGaAsP membrane is released from the substrate by wet etching in 4:1 HCl:water solution at 4^oC. The final structure is a free standing membrane supported at one side (Figure 5).

Each pattern shown in Figure 5(a) consists of six different cavities that have received the same electron-dose

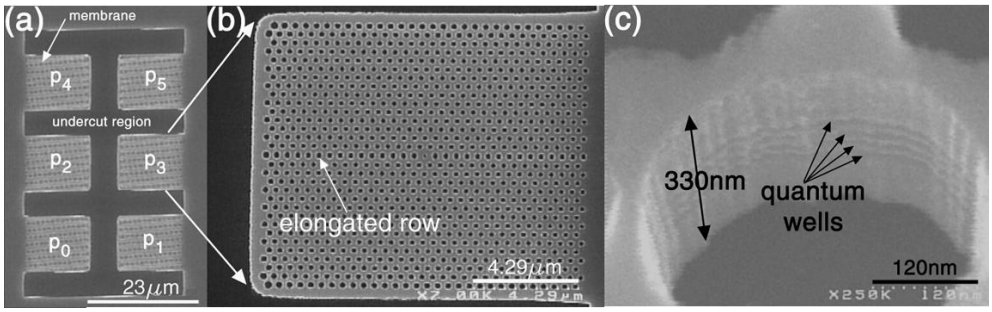

Figure 5. SEM micrograph of the structure b_4. Each structure consists of (a) six different cavities with different elongation parameters: $p_0 = 0$, $p_1 = 0.05 \cdot a$, $p_2 = 0.1 \cdot a$, $p_3 = 0.15 \cdot a$, $p_4 = 0.2 \cdot a$ and $p_5 = 0.25 \cdot a$. (b) Blow-up of p_3 cavity, and (c) of a single hole (tilted). Quantum wells and undercut air region can be seen.

during the e-beam lithography step, and therefore should have similar hole size (r) and lattice constant (a). The only difference between the cavities in one structure is the value of the dislocation parameter p that assumed values in the range $p/a \in (0, 0.25)$. In our experiments we tested several structures, but in this work we report results for three structures (each of them consists of six different cavities). The structures are labelled a_2, b_1 and b_4, according to their position within 5x10 matrix of fabricated structures. In Figure 6 we show scanning electron microscopy (SEM) micrographs of four cavities that lased, as described in the following section. In order to determine the exact geometry of these nano-laser, we performed detailed image-analysis of the SEM micrographs of these four cavities. We used pattern recognition procedure to determine the area of *all* holes that make photonic crystal mirrors, and to estimate the radius of each hole. The results are shown in Figure 6 and summarized in Table 1.

Table 1. Table 1 - Geometry of four nano-lasers tested in the experiment

	r	r/a	r_{def}	r_{def}/a
a_2, p_4	126nm	0.290	≈50nm	0.115
b_1, p_5	125nm	0.290	≈71nm	0.162
b_4, p_5	139nm	0.320	≈73nm	0.168
b_4, p_4	138nm	0.317	≈73nm	0.168

Due to problems with the PMMA mask used, quality of fabrication procedure deteriorated when the patterns were transferred from PMMA into the metal layer. However, even though holes are "funny" shaped, the effective radius is very uniform and the hole radius variation is better than $\pm 5nm$. In case of b_4 structure, that we show the most experimental data for in the following section, the average hole size is found to be $r \approx 140$nm, and average periodicity of the photonic crystal lattice $a = 435nm$. This combination of geometries yield relative thickness of $d/a = 0.76$ and relative hole size $r/a = 0.32$. This is slightly different geometry than the one we

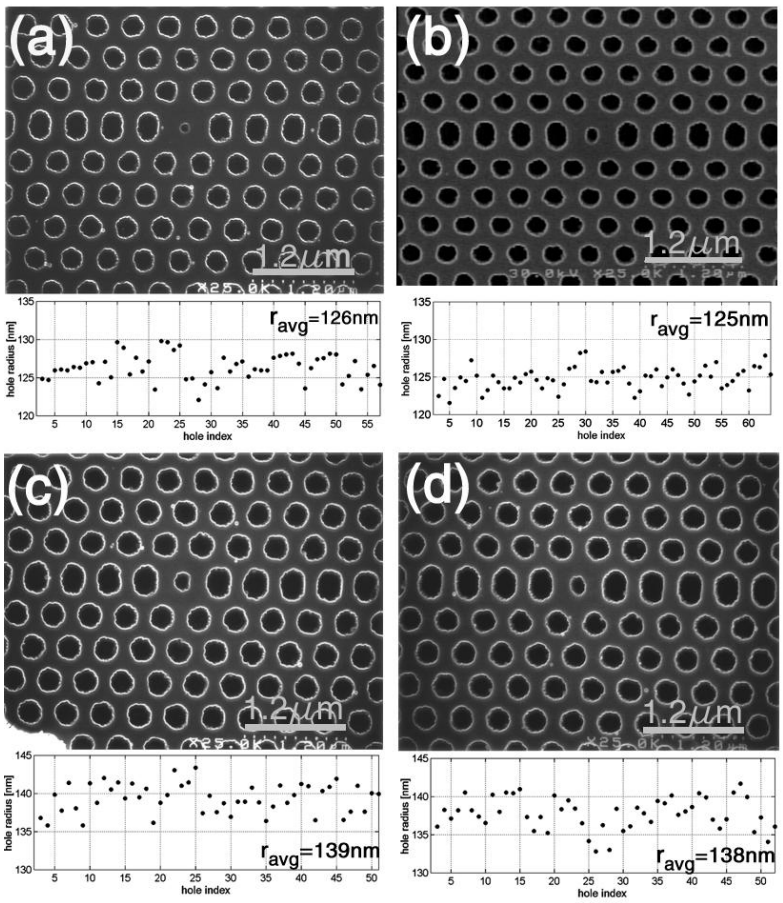

Figure 6. SEM micrographs of (a) $a_2\ p_4$, (b) $b_1\ p_5$, (c) $b_4\ p_4$ and (d) $b_4\ p_5$ along with the distribution of hole sizes in the bulk photonic crystal mirrors surrounding each cavity.

analyzed in the Section II. Using 3D FDTD code we found that for this geometry photonic bandgap is located in the range $a/\lambda = (0.253, 0.345)$. Due to increased hole size, Q-factors of fabricated structures are expected to be smaller than those reported in previous section. Moreover, Q-factors are expected to be even further decreased due to increased scattering of light at the rugged hole walls (Figure 6).

4. EXPERIMENTAL RESULTS

Our cavities were optically pumped using a laser source at $\lambda = 830$nm. Heat-sinking was poor in our structures, since they are defined in the membrane that is connected to the substrate at one side only. Therefore, in order to prevent overheating of the lasers, we pumped them in pulsed regime. In most of the cases structures were pumped with 10ns long pulses,[18] with periodicity $1\mu s$, yielding the duty cycle of $DC = 1\%$. Schematic of the setup used in the experiment is shown in Figure 7. The pump beam was focused through 100x objective lens onto the sample surface to obtain a spot size of about $3\mu m$. The emission from the cavities was collected through the same lens, and the spectrum of the emitted light signal was detected with an optical spectrum analyzer (OSA). An additional flip-up mirror was used to obtain the optical images of the excitation pump-spot and the cavity modes.

As the first step we measured the emission from the unprocessed InGaAsP material and obtained the gain spectrum of the active material. We found that emission exists between 1300nm and 1650nm, with a maximum

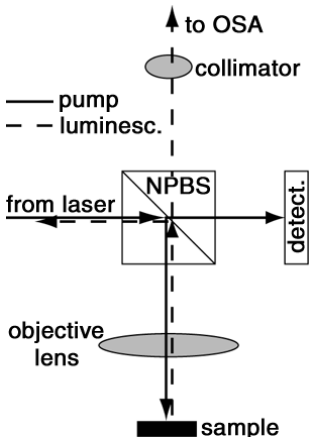

Figure 7. Experimental setup. NPBS stands for Non-polarizing beam splitter.

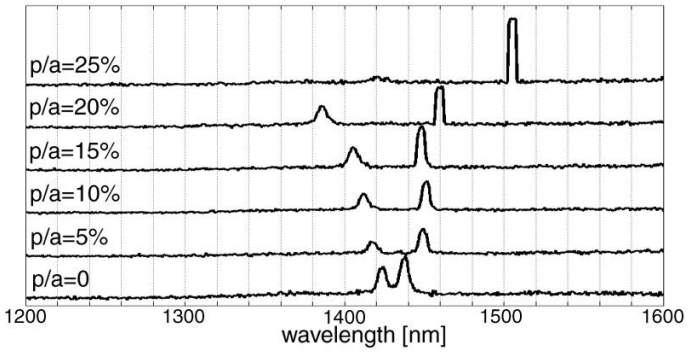

Figure 8. Structure b_4. Position of resonant modes detected in cavities $p_0 \div p_5$ as a function of the elongation parameter p.

at around 1550nm. This wavelength range corresponds to normalized frequencies of $a/\lambda \in (0.264, 0.335)$, which is within the bandgap of the bulk photonic crystal mirrors surrounding the cavity. Next, we tested all six cavities in b_4 structure in order to characterize their resonant modes. We found two prominent resonant peaks in the emission range of our InGaAsP material (Figure 8), and we observed that the position of these resonances depends strongly on the value of the elongation parameter p, as predicted by our theoretical calculations (Figure 3). Originally double degenerate modes of a single defect cavity with no dislocations introduced (p_0) become split apart as dislocation is introduced, and the splitting between two modes increases as amount of dislocation increases. LQ mode positioned at higher frequencies (shorter wavelength) is shifted towards shorter wavelengths, while HQ mode is shifted towards longer wavelengths, as we increase dislocation. This is in very good agreement with theoretical predictions of Section II. Slight variations observed in the case of structure p_5 (peaks jump towards longer wavelengths) might be attributed to the non-uniform defect hole size. Indeed, as we observed in Section II, positions of peaks are strongly dependent on the defect hole size. In addition, LQ and HQ modes are split even in the case of p_0. We have attributed this to the broken symmetry of the structure due to the fabrication disorders.

By introducing polarizer between the non-polarizing beam splitter (NPBS) and the collimator (Figure 7) we could select polarization of the photoluminescence signal, and investigate polarization properties of the LQ and HQ modes. We observed that these two modes are linearly polarized, but have orthogonal polarization (Figure 9). This is in an excellent agreement with our 3D FDTD analysis that shows that LQ mode is polarized along y-axis direction, while HQ mode is polarized along x-axis direction.

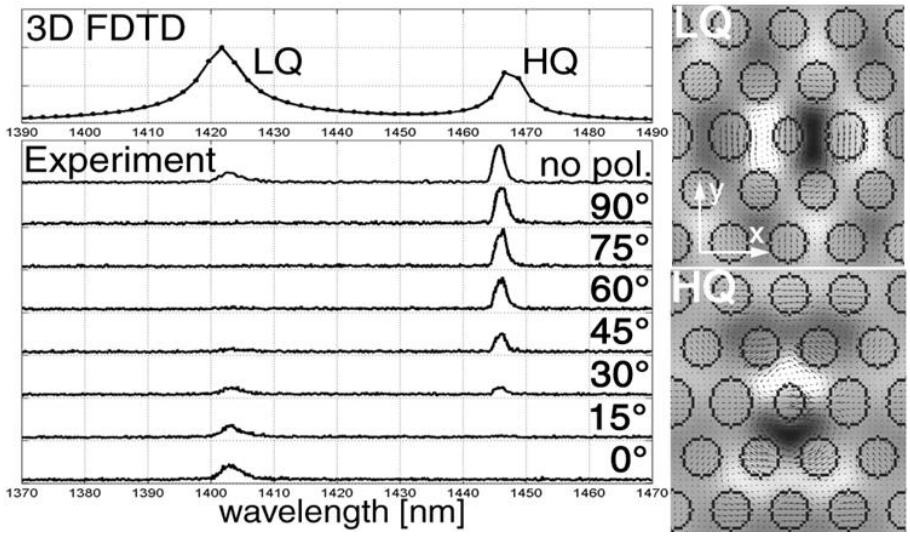

Figure 9. Structure b_4, cavity p_3. Polarization dependance of the resonant modes. 0^o corresponds to y-axis direction. Figure also shows mode profiles (B_z component), polarization ($\vec{E}$) and position in the spectrum of the LQ and HQ modes, the result of 3D FDTD analysis.

In Figure 10 we show the dependence of detected peak output optical power as a function of peak input

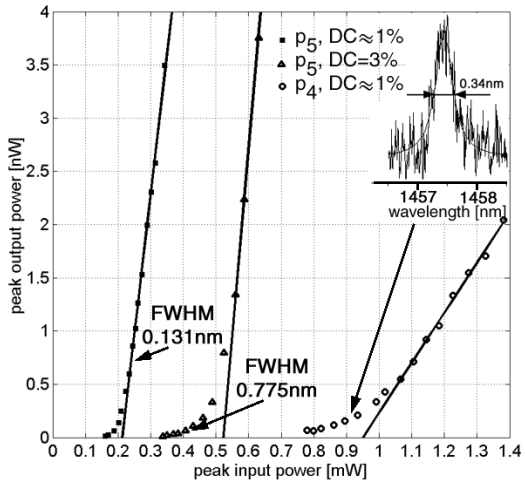

Figure 10. Structure b_4. L-L curve for p_5 and p_4 cavities for two different duty cycles (DC). The pulse periodicity was $1\mu s$ in both cases. Spectrum taken below threshold, in the case of p_4 cavity is shown in the inset.

optical power (L-L curve) for HQ resonant mode of p_4 and p_5 cavities in structure b_4. In the case of structure p_5 pumped with 1% duty cycle threshold power as low as $P_{th} = 214\mu W$ is observed. This threshold power go up to $520\mu W$ when duty cycle is increased to 3%. We have attributed this increase in the threshold power to poor heat dissipation of our nano-laser and its increased temperature. Quality factor in the case of p_5 structure was estimated from below threshold luminescence measurements to be around $Q \approx 2,000$ (Figure 10). However, it should be mentioned that by estimating Q factors of the cavity from below-threshold characteristics, we underestimate actual Q-value. This is due to additional losses introduced in the cavity due to the re-absorption of

light in the active region (quantum wells). Therefore, we expect actual Q-values to be higher and in the range of $6,000$ as predicted by theory. In Figure 10 we also show L-L curve for p_4 cavity in the b_4 structure. It can be seen that threshold is higher in this case, and it is around $P_{th} = 950\mu W$. There are several reasons for increased threshold: gain provided from quantum wells is smaller at this wavelength ($\lambda = 1457.5$nm) than in the case of p_5 cavity ($\lambda = 1504$) since gain peaks at $\lambda \approx 1550$nm; second, for $r_{def} \approx 0.15a$ Q factor of p_4 cavity is smaller than Q factor of p_5, as shown in Section II; finally, p_5 structure has more dielectric material in the cavity region (bigger dislocation), and the mode-overlap with the gain material is better than in the case of p_4 structure.

In the inset of Figure 10 we show spectrum of the HQ peak of the p_4 cavity (set b_4), taken at the threshold. Full-width half-maximum of the resonance is $FWHM = 0.34$nm, and that corresponds to Q factor of $Q \approx 4,300$. This is in good agreement with our theoretical predictions of $Q_{p4} = 4,000$. However, since the spectrum is taken at the threshold, it is possible that the linewidth is narrowed due to the presence of the gain. Therefore, this very high Q value that we measure should be taken with caution, and more detailed analysis is to be conducted in order to get reliable estimates for Q-factors. For example, structures defined in passive materials (e.g. SOI) should be characterized in order to get unambiguous estimates of Q-factors.

In order to further reduce threshold powers, it is beneficial to make structures with smaller holes since that improves Q-factors. Also, the defect hole should be smaller in order to increase mode overlap with the dielectric (gain) material. As it can be seen in Table 1, cavity p_5 from set b_1 satisfies these conditions. Therefore, we expect to observe small threshold power in the case of this cavity. In Figure 11 we show the positions of the resonant modes in the cavity b_1 p_5. The spectra are taken for two different pumping level, and line-narrowing can be observed as laser is pumped harder. It can be seen that HQ resonance is positioned at $\lambda = 1560$, almost exactly at the position of the maximum gain ($\lambda = 1550$nm). Q-factor of the LQ mode was estimated to be $Q_{LQ} = 505$. In Figure 12 we show L-L curves for this structure, taken for two different pumping levels. It can be seen that threshold power in this structure is smaller than in the case of structure b_4p_5 shown in Figure 10.

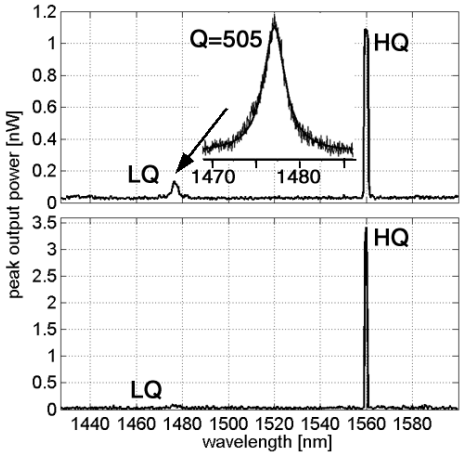

Figure 11. Structure b_1, cavity p_5. Photoluminescence spectra taken at two different pumping levels. Narrowing of the linewidth in case of HQ mode can be observed. Q-factors of LQ mode are estimated to be around $Q_{LQ} = 505$.

In Figure 13 we show L-L curve for a_2 p_4 cavity, as well as tuning characteristics of structure a_2. This cavity also supports two modes, and the one at longer wavelength (HQ mode) lases. Since both holes in the bulk photonic crystal mirror surrounding the cavity and the central defect hole are smaller in this case (Table 1), resonances are shifted towards longer wavelengths (smaller energies). A photoluminescence spectrum taken above threshold, as well as the mode profiles taken at different pumping levels, are shown in the inset. The size of the light spot emitted from the nano-laser is on the order of $3.9\mu m^2$, a strong indication that this laser has a small mode volume. When the pump beam is only slightly moved from the center of the cavity (less than $1\mu m$), the strong light intensity shown in Figure 13 disappears. This micro-photoluminescence result is another

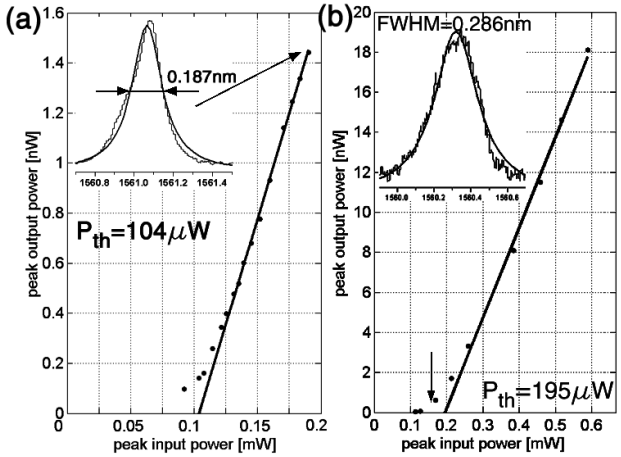

Figure 12. L-L curve of structure b_1 p_5 taken at different pumping levels. $DC = 1\%$

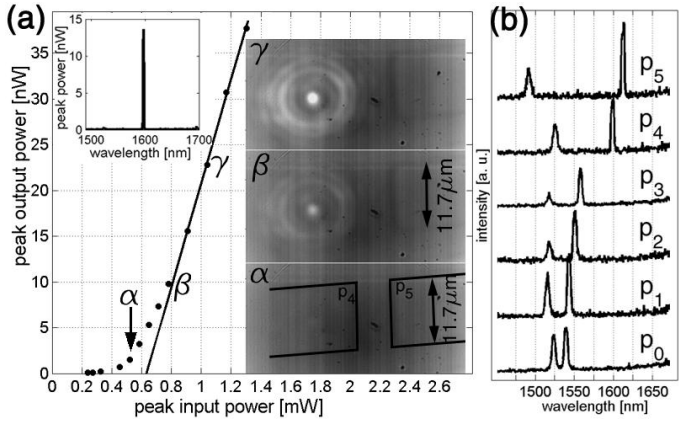

Figure 13. Structure a_2 p_4. (a) L-L curve. Lasing action occurs from HQ mode positioned at $\lambda = 1598nm$. Insets show spectrum above threshold, and mode profiles of the lasing mode for several pump levels. The boundaries of the structure can also be seen. The mode is very well localized to the center of the cavity. (b) Tuning properties of a_2 structure, as a function of elongation parameter p.

confirmation that we indeed observe lasing from a well localized, small mode volume, high Q resonant mode.

5. DISCUSSION AND CONCLUSIONS

We have fabricated and characterized photonic crystal nano-cavities based on our fractional edge dislocations design. We have numerically modelled our cavities and have investigated dependence of the optical properties of the cavities on their geometry. The cavities were fabricated in active InGaAsP material, in a free-standing membrane planar photonic crystal platform. The structures were tested at room temperature, and were optically pumped with pulsed laser source. Lasing was observed from the high-Q dipole modes of the cavities. In spite of the unusual design of our structures, which has a hole etched through the position of maximum field intensity, we observed low threshold powers in our devices. We have attributed this to the small mode volume and the high Q factors inherent to our device design. In addition, low-Q dipole mode, positioned at shorter wavelengths, was experimentally characterized and results are in good agreement with finite difference time domain model predictions. Polarization and lithographic tuning properties of high- and low-Q modes are also

in an excellent agreement with theoretical FDTD predictions. The mode profiles taken by our IR camera show that the lasing resonance is well localized to the center of our cavity. Based on these experimental results, we conclude that the observed room temperature lasing action corresponds to the high Q mode of our nano-cavity.

6. ACKNOWLEDGEMENTS

This work was supported by the Caltech MURI Center for Quantum Networks and NSF. The authors would like to acknowledge discussions and interactions with Prof. Jelena Vučković (Stanford University) and Prof. Hideo Mabuchi (Caltech). The JPL authors would like to acknowledge the partial support from the Cross Enterprise Technology Development Program at Jet Propulsion Laboratory (under a contract with the National Aeronautics and Space Administration).

REFERENCES

1. T. F. Krauss, R. M. De La Rue and S. Brand, "Two-dimensional photonic-bandgap structures operating at near infraed wavelengths", *Nature*, **383**, pp. 699-702 (1996).
2. S. G. Johnson and S. H. Fan and P. R. Villeneuve and J. D. Joannopoulos and L. Kolodziejski, "Guided modes in photonic crystal slabs", *Phys. Rev. B*, **60**, pp. 5751-5758, (1999).
3. O. Painter, J. Vučković and A. Scherer, "Defect modes of a two-dimensional photonic crystal in an optically thin dielectric slab", *JOSA B*, **16**, pp. 275-285 (1999).
4. E. Miyai and K. Sakoda, "Localized defect modes with high-quality factors in a photonic crystal slab on a low-index dielectric substrate", *Jap. J. of Appl. Phys.*, **41**, pp. L694-L696, (2002)
5. J. Vučković, M. Lončar, H. Mabuchi and A. Scherer, "Design of photonic crystal microcavities for cavity QED", *Phys. Rev. E.*, **65**, 016608 (2001).
6. H. Y. Ryu, H. G. Park, Y. H. Lee, "Two-dimensional photonic crystal semiconductor lasers: Computational design, fabrication, and characterization", *IEEE J. of Sel. Top. in Quant. Elect.*, **8**, pp. 891-908 (2002).
7. S. G. Johnson, S. Fan, A. Mekis and J. D. Joannopoulos, "Multipole-cancellation mechanism for high-Q cavities in the absence of a complete photonic band gap", *Appl. Phys. Lett.*, **78**, pp.3388-3390 (2001).
8. T. Yoshie, J. Vučković, A. Scherer, H. Chen and D. Deppe, "High quality two-dimensional photonic crystal slab cavities", *Appl. Phys. Lett.*, **79**, pp. 4289-4291 (2001).
9. O. J. Painter, A. Husain, A. Scherer, J. D. O'Brien, I. Kim and P. D. Dapkus, "Room temperature photonic crystal defect lasers at near-infrared wavelengths in InGaAsP", *J. of Lightw. Tech.*, **17**, pp. 2082-2088 (1999).
10. H. G. Park, J. K. Hwang, J. Huh, H. Y. Ryu and Y. H. Lee, "Nondegenerate monopole-mode two-dimensional photonic band gap laser", *Appl. Phys. Lett.*, **79**, pp. 3032-3034 (2001).
11. P. T. Lee, J. R. Cao, S. J. Choi, Z. J. Wei, J. D. O'Brien and P. D. Dapkus, "Room-temperature operation of VCESL-pumped photonic crystal lasers", *IEEE Phot. Tech. Lett.*, **14**, pp. 435-437 (2002).
12. H. Y. Ryu, S. H. Kim, H. G. Park, J. K. Hwang, Y. H. Lee, "Square-lattice photonic band-gap single-cell laser operating in the lowest-order whispeing gallery mode", *Appl. Phys. Lett.*, **80**, pp. 3883-3885 (2002).
13. C. Monat, C. Seassal, X. Letartre, P. Viktorovitch, et al., "InP 2D photonic crystal microlasers on silicon wafers: room temperature operation at $1.55\mu m$", *Elec. Lett.*, **37**, pp. 764-766 (2001).
14. M. Lončar, T. Yoshie, A. Scherer, P. Gogna and Y. Qiu, "Low-threshold photonic crystal laser", *Appl. Phys. Lett.*, **81**, pp. 2680-2682 (2002).
15. R. K. Lee, O. J. Painter, B. Kitzke, A. Scherer and A. Yariv, "Photonic bandgap disk laser", *Elect. Lettl*, **35**, pp. 569-570 (1999).
16. J. Vučković, M. Lončar, H. Mabuchi and A. Scherer, "Optimization of the Q factor in photonic crystal microcavities", *IEEE J. of Quant. Elect.*, **38**, pp. 850-856 (2002).
17. M. Lončar, T. Doll, J. Vučković and A. Scherer, "Design and fabrication of photonic crystal waveguides", *J. of Lightw. Tech*, **18**, pp. 1402-1411 (2000).
18. Effective pulse width can be smaller than 10ns (yielding smaller effective duty cycles) due to the finite rise time of pulse generator.